Journal of Power Sources 255 (2014) 450–458

Contents lists available at ScienceDirect

Journal of Power Sources

journal homepage: www.elsevier.com/locate/jpowsour

Calendar aging of commercial graphite/$LiFePO_4$ cell – Predicting capacity fade under time dependent storage conditions

Sébastien Grolleau [a,b,*], Arnaud Delaille [a], Hamid Gualous [b], Philippe Gyan [c], Renaud Revel [d], Julien Bernard [d], Eduardo Redondo-Iglesias [e], Jérémy Peter [e], On behalf of the SIMCAL Network

[a] Laboratory for Electrical Storage (CEA/LSE), CEA-LITEN-DTS, 73377 Le-Bourget-du-Lac, France
[b] LUSAC ESIX Normandie rue Louis Aragon, 50130 Cherbourg-Octeville, France
[c] DREAM/DELT'A/68580, TCR LAB 012, 1, Avenue du Golf, 78288 Guyancourt Cedex, France
[d] IFP Energies Nouvelles, Etablissement de Lyon, BP 3, 69360 Solaize, France
[e] IFSTTAR/LTE, Cité des Mobilités, 25 Av Francois Mitterrand, 69675 Bron, France

HIGHLIGHTS

- C/LFP cells were submitted to 11 storage conditions during at least 450 days.
- Capacity fade rate is both SoC and temperature dependant.
- We model capacity fade based on aging results on nine static conditions.
- Life model was validated against data obtained in time varying environments.

ARTICLE INFO

Article history:
Received 5 June 2013
Received in revised form
25 November 2013
Accepted 26 November 2013
Available online 11 December 2013

Keywords:
Li-ion battery aging
$C/LiFePO_4$
Storage
Capacity fade experimental data
Capacity fade model
Time varying environment

ABSTRACT

In applications such as electrical transportation, most of the battery life is spent under storage. Understanding and estimating aging under storage, also named as calendar aging, is therefore a prerequisite for cell life prediction. This work investigates aging behavior upon storage of a commercial 15 Ah lithium-ion graphite/iron phosphate cell. Performance decline during 450 days of storage under nine stationary conditions is analyzed using non-destructive electrochemical tests. Temperature is found to be more detrimental than State of Charge (SoC). Most often, degradation models express the accumulated degradation with respect to time and aging conditions. In this article, a simple modeling approach is proposed focusing on the degradation rate to predict capacity fade. This permits predicting cell degradation under time dependent storage conditions (SoC and temperature) which are usually experienced in real applications. Model prediction is compared to experimental calendar aging data obtained over 625 days in a controlled time dependent temperature storage conditions. Predictions are in good agreement with experimental results as the absolute error on capacity prediction never exceeds 3% over 400 days and 5% over 625 days.

1. Introduction

Lithium-ion battery (LIB) technology is a promising candidate for automotive applications due to their impressive energy and power densities. However, long cell lifetime required for these applications (up to 15 years) is still uncertain for LIBs.

LIB performances decline over time as a consequence of diverse physical aging causes that depend on electrode and electrolyte used. Aging occurs during both cycling and storage mode. Considering that a personal car spends about 95% of its life in parking mode, the study of lithium-ion battery aging during storage seems particularly relevant.

Many studies about lithium-ion battery aging during storage can be found in the literature [1–7]. During storage, lithium-ion batteries like other chemical storage systems experience capacity loss which is composed of two terms, a reversible and an irreversible one. The reversible capacity loss fraction also called self-discharge

* Corresponding author. Laboratory for Electrical Storage, CEA-LITEN-DTS, 73377 Le-Bourget-du-Lac, France. Tel.: +33 4 79 79 21 71; fax: +33 4 79 68 80 49.
E-mail addresses: sebastien.grolleau@cea.fr, sebastien.grolleau@gmail.com (S. Grolleau).

0378-7753/$ – see front matter © 2013 Elsevier B.V. All rights reserved.
http://dx.doi.org/10.1016/j.jpowsour.2013.11.098

Abbreviations

BMS	battery management system
EIS	electrochemical impedance spectroscopy
EV	electrical vehicle
LFP	$LiFePO_4$
LIB	lithium-ion battery
SoC	state of charge
SoE	state of energy
SoH	state of health
SEI	solid electrolyte interface

can be recovered by fully re-charging cell after storage. Aging processes depends not only on storage conditions but also strongly on the materials used for electrodes and electrolyte [8–10].

According to [11] the numerous aging processes have three main consequences leading to cell degradation:

(i) Loss of cyclable lithium: side reactions with lithium-consumption may occur at both electrolyte/electrode interfaces (e.g., growth of passivation layers at both electrode sides due to electrolyte decomposition). If the rate of lithium consumption at the negative electrode is different from the rate at the positive, the cell experiences a loss of cyclable lithium due to an increase of the cell imbalance.
(ii) Loss of active materials (e.g., material dissolution, structural degradation, particle isolation, and electrode delamination)
(iii) Impedance increase of the cell (e.g., passive films at the active particle surface and loss of electrical contact within the porous electrode).

Nowadays, the majority of commercial lithium-ion batteries use graphite as negative electrode material. Parasitic reactions occurring at negative electrode/electrolyte interface seems to play a major role in LIBs degradation and have been intensively studied [12–14]. Although Solid Electrolyte Interface (SEI) proposed by Peled et al. [15] plays a protecting role as it prevents the graphite from further electrolyte degradation, continuous growth of the SEI layer is obviously detrimental to the cell performance of LIBs as lithium is irreversibly consumed and may cause an increase of the overall cell resistance. Moreover, when the SEI layer becomes too thick, some portion of active material can become electrochemically inactive leading to active material loss of carbon negative electrode [16].

All studies demonstrate that, high temperatures are more detrimental for cell life upon storage by activating parasitic reactions. SoC influences also cell degradation during storage but to a lesser extent; fully lithiated graphite is indeed considered to be unstable because the intercalated lithium tends to diffuse to the graphite edges where it may interact with the solvent components [13]. Furthermore, commercial lithium-ion cell studies demonstrated also possible interactions of positive electrode with the SEI layer. $LiMn_2O_4$ spinel and the $LiFePO_4$ (LFP) have been reported to release transition metals (Mn^{2+}, Fe^{2+}) that can be reduced on negative side and incorporated into the anode SEI which leads to catalytic effect accelerating cell degradation [6,8].

Since its introduction in 1997 by Padhi [17], LFP based cells have attracted significant interest for automotive application as a cathode material for LIBs. Indeed, it constitutes a low cost material with excellent safety characteristics and it has the potential of providing a long cycle and calendar life due to the relative stable and safe olivine chemistry structure.

Cycling induced aging of graphite/LFP cells has been intensively reported [6,16,18–20]. An empirical cycling model has been proposed for a commercial 2.3 Ah graphite/LFP cell [21]. Their results suggest that capacity loss is mainly affected by exposure time and temperature but calendar aging has not been considered. In previous work [11], authors reported on one year aging both under cycling and under storage at 25 °C and 45 °C. Extent of capacity fade is larger for cells under cycling in comparison with cells under storage for the same aging time. Post-mortem analysis [22,23] reveal that for both storage and cycling conditions, aging is dominated by the loss of cyclable lithium due to the growth of the SEI layer at the graphite electrode. Degradation of the carbon negative electrode was only observed for long-term cycling at elevated temperature.

As most of the battery life is spent under storage in applications such electric vehicles (EV), predicting aging under storage is a prerequisite for life evaluation. Ability to simulate battery performance and aging under different modes of operation (both storage and cycling) is highly desired for the purpose of battery-life prediction. Moreover, life predicting models are required not only for the optimal design of the battery but also for onboard battery management systems (BMS) during its operation in an EV.

This study presents calendar aging results on a commercial energy-designed 15 Ah graphite/LFP cell and proposes in a second part an empirical model for estimating capacity decline over time. Finally, model predictions are compared with experimental aging data upon storage acquired in a variable temperature environment on the same cells.

2. Experimental

Experiments were conducted on 33 similar commercial cylindrical 15 Ah graphite/LFP cells. Electrochemical characterization tests were performed using multipotentiostats (VMP3, BioLogic) connected with 20 A boosters except for tests performed at laboratory CEA/LSE (VersaSTAT MC, Princeton Applied Research). The electrolyte composition details of this cell are not known. The cell ratings given by the cell manufacturer are summarized in Table 1.

Before characterizing their initial performance, the cells were preconditioned by applying 6 charge/discharge full cycles in order to remove possible outlier cells. Thereby, a constant current corresponding to the nominal rate of the cell ($1C_{nom} = 15$ A) has been applied until cell potential reached 2.00 V, followed by 30 min rest. Then, cells were charged with a classical Constant Current–Constant Voltage (CC–CV) charge up to 3.65 V and potential was held at 3.65 V until a cut-off current $|I_{cut\text{-}off}| = C_{nom}/20$ followed by another 30 min rest period. The measured capacity of this cell at $1C_{nom}$ was 14.8 Ah at 25 °C with a standard deviation of around 0.3 Ah.

2.1. Tests conditions

Two parameters have been investigated: the State of Charge (SoC) and the temperature of storage. Three SoC and three temperatures are considered: 30%, 65%, 100%, and 30 °C, 45 °C, 60 °C respectively, as indicated in the test matrix on Table 2. Laboratories where the aging tests and the aforementioned preconditioning

Table 1
Cell ratings.

Parameter	Value
Nominal capacity at $1C_{nom}$, 25 °C (Ah)	15
End of discharge voltage (V)	2.00
End of charge voltage (V)	3.65
End of charge current (A)	0.75

Table 2
Test matrix. Each entry corresponds to a set of storage condition (temperature and SoC). An index is also provided to identify each aging test condition.

Temperature (°C)	SoC (%)		
	30%	65%	100%
30°C	IFSTTAR/LTE (1)	IFSTTAR/LTE (2)	IFSTTAR/LTE (3)
45 °C	IFP Energies Nouvelles (4)	IFP Energies Nouvelles (5)	IFP Energies Nouvelles (6)
60 °C	CEA/LSE (7)	CEA/LSE (8)	CEA/LSE (9)
30//45 °C	CEA/LSE (10)	Not tested	CEA/LSE (11)

tests were conducted are also indicated. After preconditioning tests and before been initially characterized, cells were stored at low temperature (<10 °C) and at medium SoC. Initial performance of the cells was performed in approximately the same timing – within two months – in test laboratories.

At each SoC/temperature, 3 cells are studied in order to avoid errors and to characterize possible discrepancy of behavior. In addition, it allows the removal of cells at the middle and at the end of the aging tests for post-mortem characterizations [23].

Besides cells stored in static storage conditions, two groups of three same technology cells were stored in a variable temperature climatic chamber (KBF 720, Binder). The temperature profile variation between 30 °C and 45 °C was repeated daily (Fig. 1). The two cell groups were respectively stored fully charged (SoC = 100%) and at SoC = 30%. These additional tests were conducted at the CEA/LSE laboratory. Results of aging of high power lithium batteries submitted to variable environments are relatively scarce in the literature. Hence, very few confrontations of simulation results with experimental values obtained in variable environments have been proposed so far.

During storage, cells were disconnected, thus cell voltage is free to evolve during storage. Periodically, performance degradation of the cells over aging was evaluated using non-destructive electrochemical methods aiming to estimate cell capacity and cell resistance. More than 450 days of storage were achieved for all test conditions.

2.2. Performance characterization

Periodical electrochemical characterizations of the cells were performed at 25 °C. The time to reach temperature equilibrium was assumed to take less than six hours. Periodicity of characterization tests has been set to 2 months for storage temperature of 30 °C and 45 °C, and shortened to 1-month for experiments at 60 °C as aging is expected to be more severe.

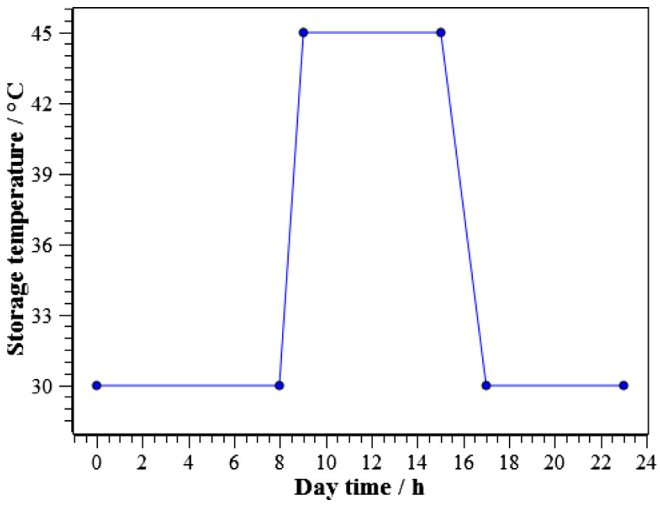

Fig. 1. Daily repeated temperature profile for dynamic storage conditions.

First of all, three discharge/charge cycles at $1C_{nom}$ at 25 °C were performed in order to measure the remaining capacities of the cells. During storage, cells experienced indeed self-discharge which means that a substantial part of the capacity loss can be recovered after a full charge using the CC–CV protocol defined above. Therefore, consecutive discharge/charge cycles are necessary to unfold the reversible and irreversible part of the capacity loss. The measured capacity which only includes the irreversible loss is named as the irreversible capacity. The State of Health (SoH) refers to the loss of irreversible capacity upon cell aging and is defined as follows:

$$\mathrm{SoH} = \frac{Q_{\mathrm{cell}}(t)}{Q_{\mathrm{cell}}(t_0)} \tag{1}$$

where $Q_{cell}(t)$ and $Q_{cell}(t_0)$ are respectively the cell irreversible capacity measured by fully discharging at $1C_{nom}$ = 15 A rate after a storage period of t days and the cell total capacity measured during the initial electrochemical test before storing cells. Alternatively, the State of Energy (SoE) is also used in this paper, which refers to the loss of available total energy during a discharge and is defined as follows:

$$\mathrm{SoE}(t) = \frac{E_{\mathrm{cell}}(t)}{E_{\mathrm{cell}}(t_0)} \tag{2}$$

where $E_{cell}(t)$ and $E_{cell}(t_0)$ are respectively the cell total energy measured after a storage period of t days and the cell total energy before storing cells. The total energy E_{cell} is measured by integrating the instantaneous electrical power supplied by the cell during the full discharge. Hence, SoE encapsulates both capacity loss and additional power loss due to internal resistance increase.

In addition, cell resistance was evaluated at different nominal SoC using discharge current pulses (at SoC = 100%, 80%, 60%, 40%) and charge current pulses (at SoC = 20%, 40%, 60%, 80%). Intensities of current pulses are set to $-1C_{nom}$ (discharge) and $1C_{nom}$ (charge). Each consecutive current pulse lasts 720 s. Discharge pulse resistance is classically defined as:

$$R_{\mathrm{p}} = \frac{V_t - V_0}{I} \tag{3}$$

where V_t–V_0 is the potential difference caused by the current pulse at a specified time t and I is the algebraic value of the current intensity ($-1C_{nom}$ = 15 A). In this work, a 10 s pulse resistance was considered as depicted by Fig. 2.

Discharge pulses were separated by a 30 min pause followed by an Electrochemical Impedance Spectroscopy (EIS) measurement whereas charge pulses are only separated by a 30 min rest.

At the end of each performance characterization test, a $1C_{nom}$ discharge was applied to the fully charged cells in order to reset the SoC before storage, during either 21 min or 42 min for SoC = 65% and 30%, respectively.

2.3. Modeling of experimental data

Since SEI formation appears to be the dominant aging source, the majority of phenomenological models are based on SEI continuous growth responsible for cyclable lithium consumption especially upon storage. In order to simplify the problem, some authors consider an only kinetic-limited mechanism considering

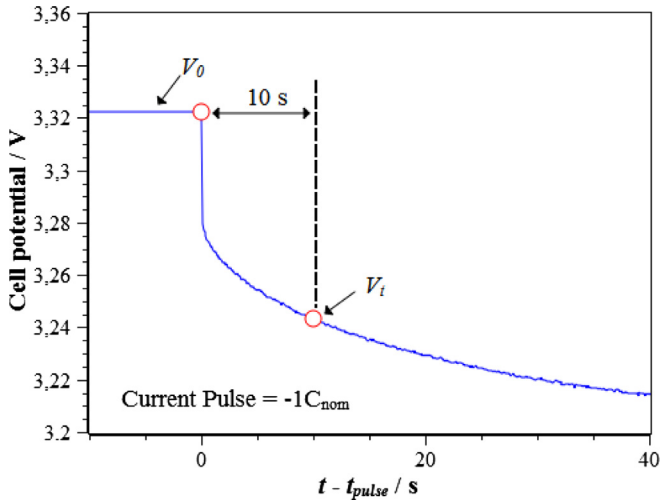

Fig. 2. Potential evolution of a fresh cell caused by a $-1C_{nom}$ discharge peak.

reactant species are provided in excess [24,25] and others consider diffusion-limited mechanism where transport of reactant through the SEI is the rate determining step [2,26,27]. Detailed modeling work compared to experimental data suggested that the reaction upon storage is more under diffusion control than under kinetic control [28]. However, depending on the assumptions made, these approaches require a detailed physic-based battery model and agreement between lifetime predictions of such model and experimental aging data over a wide range of conditions have not been proposed so far.

On the other hand, a wide variety of empirical degradation models have been proposed so far in the literature for performance prediction. Some of them are purely empirical without making any assumption on the underlying aging mechanisms [29–31]. Alternatively, exponential relations have been also suggested to model SEI growth [7]. Cell degradation (resistance increase or capacity retention) is expressed as a relation between stress level and exposure time. For models predicting degradation under storage conditions, temperature is commonly taken into account using an Arrhenius law. SoC of storage is more rarely taken into account as it is often observed as having minor influence.

These models are often proposed in a capacity loss cumulative form deduced form experimental data obtained under constant stress conditions (temperature and SoC); however, in real applications such as electric transportation, stress conditions are far from being constant over time. Therefore, it is highly valuable to develop models based on the degradation rate which permit predicting degradation under non-constant stress levels conditions as suggested by Thomas et al. [32].

In this work, a simple empirical expression for predicting capacity fade is proposed:

$$\frac{dQ_{loss}}{dt} = k(T,SoC)\cdot\left(1+\frac{Q_{loss}(t)}{C_{nom}}\right)^{-\alpha(T)} \quad (4)$$

with:

- $k(T,SoC)$ is the kinetic dependence of the capacity fade evolution with T and SoC during storage. Its expression is determined in the Section 3.2.
- $Q_{loss}(t)/C_{nom}$ is the fractional capacity loss at aging time t.
- the term $(1+Q_{loss}(t)/C_{nom})^{-\alpha(T)}$ with $\alpha(T)>0$ can be related to the diffusion limitation of solvent molecule inside the SEI layer which tends to decrease the capacity fade rate. Transport properties of solvent molecule through SEI layer are temperature dependent [22].

Setting $\alpha = 1$ and integrating Eq. (4) with $Q_{loss} = 0$ at $t = 0$ lead to the equation:

$$Q_{loss}(t) + \frac{1}{2}\cdot\frac{Q_{loss}(t)^2}{C_{nom}} = k(T,SoC)\cdot t \quad (5)$$

This equation is similar to the equation proposed by Broussely et al. [2] to describe capacity loss of lithium-ion cells on calendar aging where a parabolic relation ($t^{1/2}$ evolution) between aging time and loss of lithium was observed. However, using this equation lead to rather poor quality fit with reported data. Although it has no real physical meaning, tuning the α value of Eq. (4) permits fitting with good agreement the capacity decay with time. The model proposed here is therefore more flexible as it can also match aging data where a strict $t^{1/2}$ evolution is not observed which is the case for reported data.

The proposed rated model is motivated by observing a decreasing rate of degradation with SoH. Integrating (5) assuming T and SoC remain constant, it comes:

$$t = \frac{C_{nom}}{(\alpha+1)\cdot k(T,SoC)}\cdot\left\{\left(1+\frac{Q_{loss}}{C_{nom}}\right)^{\alpha+1}-1\right\} \quad (6)$$

Numerical values of model parameters α and k can be estimated using non-linear regressions conducted on capacity loss data presented previously using Eq. (6). Non-linear regressions were performed using the *nlinfit* function from MATLAB (The MathWorks, Inc). Contrary to ordinary least-square regression, influence of possible outliers is decreased by using robust regression. The weighting function is the bisquare function with its default parameter value.

3. Results and discussion

3.1. Aging results

3.1.1. Discharge capacities

The graph on Fig. 3 displays the discharge $1C_{nom}$ capacity evolutions of the tested cells measured during periodic characterization tests. Data points of each storage condition have been linked with straight lines to improve clarity. The conventional limit of 20%

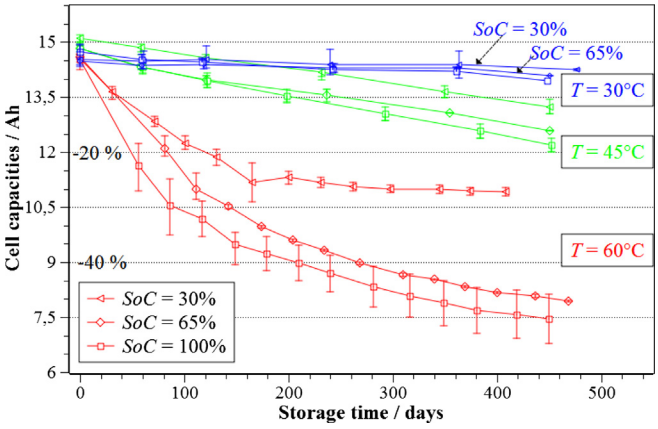

Fig. 3. Discharge capacities at $1C_{nom}$ and $T = 25$ °C of the tested cells for the 9 aging conditions. Data points of each storage condition have been linked for clarity.

capacity loss referring to the nominal capacity 15 Ah is also displayed as well as the 40% capacity loss limit. Amongst all tested cells, three exhibited a faster capacity decline comparing to the two other cells of the same batch submitted to the same aging condition. Their results are consequently not presented to avoid misinterpretation.

Storage temperature has a strong impact on capacity fade rate: cells stored at 30 °C experienced less than 10% capacity loss after 450 days of storage whereas, at 45 °C, capacity fade extents 20% for fully charged cells (SoC_{nom} = 100%). For fully charged cells stored at 60 °C, 20% capacity loss is reached in approximately 60 days only.

Cells stored at higher SoC experienced faster capacity fade. At 60 °C, a 20% capacity loss is reached in 100 days for cells stored at SoC_{nom} = 30%. Obviously, SoC influence increases with storage temperature. All capacity fades seem to follow a fairly linear evolution on the presented time frame at 30 °C and 45 °C, whereas at 60 °C capacity fade evolution is no more linear with storage time. For the cells aged under severe aging conditions (e.g., 60 °C, SoC_{nom} = 100%) dispersion in capacity is higher for aged cells compared to fresh ones, suggesting an additional dispersion due to aging.

Cells stored at T = 60 °C and SoC_{nom} = 30% exhibit a particular evolution pattern with time as cell capacities stabilize after 150 days of storage. This result must be attributable to the check-up protocol defined in Section 2.2: as the amount of discharged Ah to reset the SoC before storing cells is constant during the entire aging test, the effective storage SoC of the cells progressively decline due to progressive capacity fade. As a result, capacity fade is no more observed in this fortuitous case.

As interval between two consecutive characterization tests were reduced to one month at 60 °C, number of tests carried out on those cells were consequently doubled. Current flow during the characterization tests may cause or accelerate internal side-reactions resulting on a faster capacity decline. Considering that more than 2000 cycles can be carried out at 25 °C and at $1C_{nom}$ according to the cell manufacturer, degradation upon cycling should be rather limited before the cell reaches its End-Of-Life. However, as previous stated, effective SoC of storage is altered by our protocol which seems to have a non-negligible impact on aging. For these two reasons, influence of more frequent characterization test on capacity fade needs to be further investigated.

3.1.2. Charge/discharge curves at 25 °C

The charge–discharge curves at $1C_{nom}$ measured at T = 25 °C on a selected cell stored at 60 °C and SoC_{nom} = 100% for the three first characterization tests are presented on Fig. 4. For this severe condition, cells exhibit a very rapid capacity decline and an increase of cell resistance as cell potential becomes lower during discharge with aging. Although cell potential is obviously affected by aging, the cell resistance increase has only minor impact on the energy loss of the cell as SoE and SoH remain almost equal upon aging.

Capacity charge and discharge voltage curves measured at T = 25 °C do not reveal a major increase of resistance even for significant aging states. At $1C_{nom}$ rate, staging voltage plateaus at the graphite anode are not distinctively observed. Valuable non-destructive methods inferring aging mechanism such as differential-capacity and differential-voltage analysis are therefore not applicable for this discharging rate.

3.1.3. Pulse resistance increase

Current peaks at $-1C_{nom}$ (discharge) and at 4 different nominal SoCs (100%, 80%, 60% and 40%) are performed during characterization tests as reported in the "Experimental" Section (2.2).

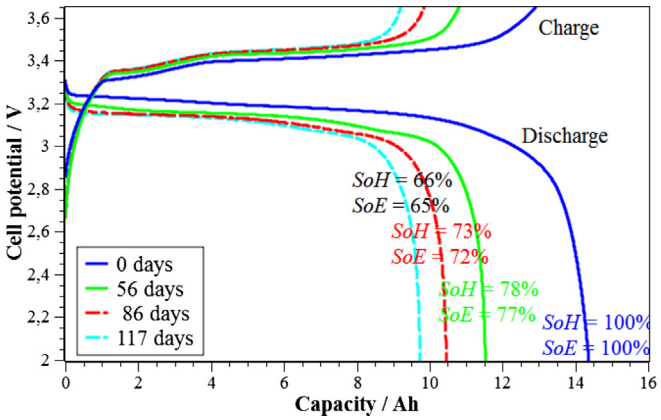

Fig. 4. Charge–discharge curves at $1C_{nom}$ measured at T = 25 °C (storage condition T = 60 °C, SoC_{nom} = 100%).

Relative variations of R_p derived from $-1C_{nom}$ (discharge resistance) current pulses at SoC_{nom} = 80% for cells stored at T = 60 °C have been averaged and are represented on Fig. 5. Although their variations exhibit a relative high spread, pulse resistances seem to increase linearly with loss of capacity for all considered conditions: the resistance increase is about 40% for a capacity loss of 15% and about 70% for a capacity loss of 40%. These results are slightly larger than other observations made on same chemistry cells submitted to calendar aging at T = 45 °C where the maximum increase of pulse resistance were less than 20% for 15% capacity loss [11] but are in the same order of magnitude of resistance increase reported for same aging conditions [5]. However, variations are much lower than drastic increase of pulse resistances measured in same conditions reported for cycling induced aging (up to 400% for only 13% capacity loss) for C/LFP based cells of different design but having a very close nominal capacity [19]. As suggested by Safari and Delacourt [11] and confirmed by post-mortem analysis [22] active material loss resulting in a decrease of the active surface area manifests by severe increase of the cell impedance. In this paper, moderate internal resistance increase is compatible with the effect of loss of cyclable lithium to SEI continuous growth that has been previously reported for this cell chemistry upon storage [5,11].

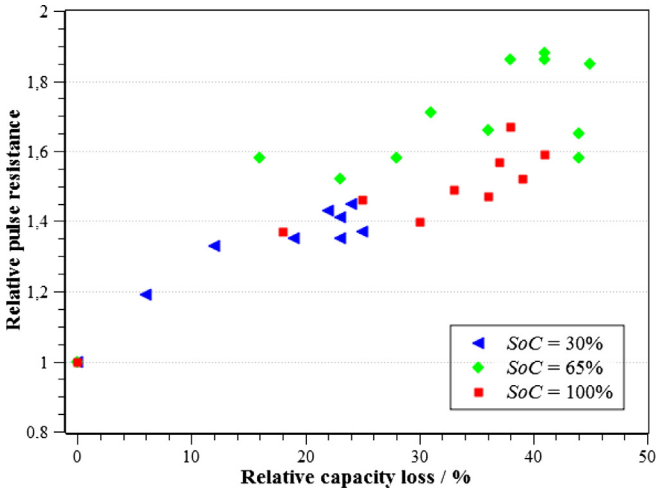

Fig. 5. Averaged pulse resistance (after 10 s discharge pulses) variations versus capacity loss for cells stored at T = 60 °C.

Table 3
Estimated α values from Eq. (6) with 95% confidence intervals.

Temp. (°C)	SoC (%)	α value estimates	Inf	Sup	Chosen α value
30 °C	30%				
	65%				3
	100%				
45 °C	30%	2.78	0.57	4.99	
	65%	1.67	0.10	3.24	3
	100%	2.92	2.18	3.66	
60 °C	30%	13.04	6.97	19.11	
	65%	7.58	6.69	8.46	7
	100%	6.03	3.86	8.20	

3.2. Capacity fade model parameters

Estimated values of α using robust non-linear regression of aging data using Eq. (6) are given in Table 3 with their 95% confidence intervals for the nine aging conditions. All estimates obtained at $T = 60$ °C are larger than those at $T = 45$ °C which tends to indicate that α increases with storage temperature. The large width obtained of confidence intervals motivates the choice of a fixed value at a given temperature. The chosen value for each temperature is given in the last column of Table 3.

For storage conditions $T = 30$ °C, the optimization routine was unable to find a good fit to data points which could be explained by the relative strong discrepancy for these conditions. Therefore, α was arbitrarily set equal to the chosen value at $T = 45$ °C and $k(T,\mathrm{SoC})$ values were adjusted manually. Data points expressed in capacity losses (Ah) of the nine cells stored at $T = 30$ °C and model fit are plotted on Fig. 6.

Once α is defined for each storage temperature, non-linear regressions of aging data are conducted again using Eq. (6) in order to obtain estimated of $k(T,\mathrm{SoC})$ plotted on Fig. 7. It appears that $k(T,\mathrm{SoC})$ follows a linear dependence with SoC whereas it increases exponentially with temperature. The following model capturing SoC and temperature dependence for $k(T,\mathrm{SoC})$ is proposed Eqs. (7)–(9):

$$k(T,\mathrm{SoC}) = A(T)\cdot\mathrm{SoC} + B(T) \tag{7}$$

$$A(T) = k_A\cdot\exp\left\{-\frac{Ea_A}{R}\cdot\left(\frac{1}{T}-\frac{1}{T_{\mathrm{ref}}}\right)\right\} \tag{8}$$

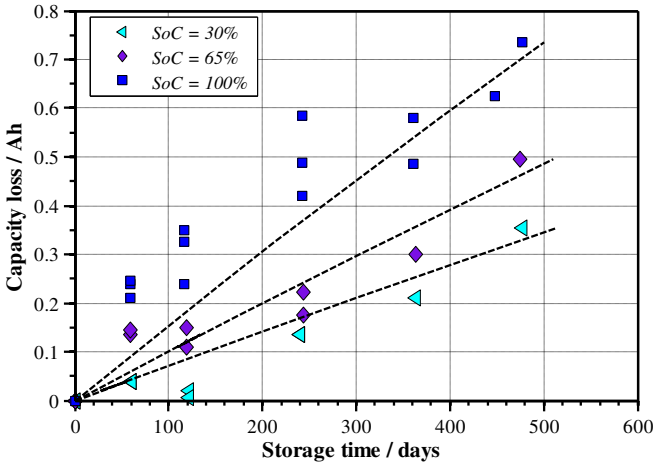

Fig. 6. Adjusted fit (broken lines) for conditions $T = 30$ °C by setting $\alpha = 3$.

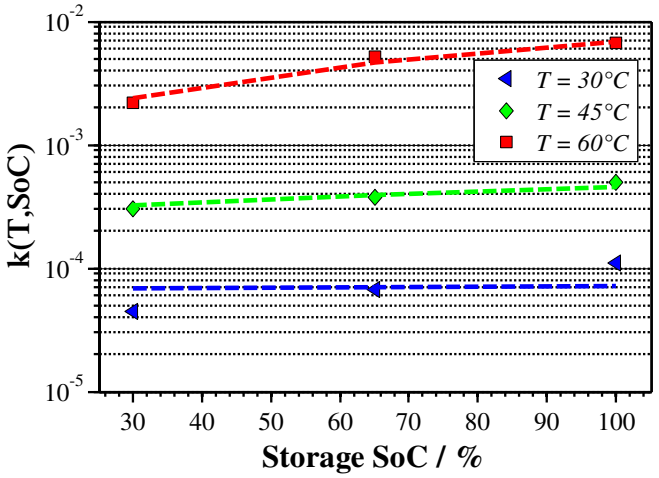

Fig. 7. Estimated $k(T,\mathrm{SoC})$ values using Eq. (5) for each storage condition. Fitted model of $k(T,\mathrm{SoC})$ using Eqs. (7)–(9) is also displayed using broken lines.

$$B(T) = k_B\cdot\exp\left\{-\frac{Ea_B}{R}\cdot\left(\frac{1}{T}-\frac{1}{T_{\mathrm{ref}}}\right)\right\} \tag{9}$$

where R is the ideal gas constant ($R = 8.314$ J mol K^{-1}). In the above expressions, T is expressed in Kelvin and T_{ref} was fixed to 298 K (25 °C) and SoC in %. Numerical values of model parameters in Table 4 were determined using the Excel solver (Microsoft) using a least squares method over all the nine conditions. Whereas model agreement is excellent for $T = 45$ °C and $T = 60$ °C, it is less optimal for the last condition. Indeed, the model predicts a quasi-constant value for k although values were significantly distinct. However, value of k at $T = 30$ °C were obtained manually and are not very precise due to the relative strong discrepancy between cells (Fig. 6).

The degradation model was simulated using Eq. (5) and compared to all aging data presented in Section 3.1.1 expressed in capacity losses on Fig. 8. A good agreement between experimental data and model prediction is observed over all the storage periods except for the condition $T = 60$ °C, $\mathrm{SoC_{nom}} = 30\%$ as the model over-predicts continuously the capacity loss after 250 days of storage (explanation given at the end of the Section 3.1.1). For the presented simulations, storage temperature and SoC of cells were considered as constant parameters. As discussed in Section 3.1.1, the effective storage SoC of the cells for conditions $\mathrm{SoC_{nom}} = 30\%$ and $\mathrm{SoC_{nom}} = 65\%$ progressively declines due to capacity fade which is not taken into account in the presented simulations.

Capacity prediction error has been calculated for each experimental data points. Distributions of prediction error expressed in % for all storage conditions are plotted on Fig. 9. On each box, the central mark is the median value of errors; the edges of the box are the 25th and 75th percentiles. The whiskers extend to the most extreme data points without considering outliers which are plotted individually (cross marker). Points are considered as outliers if they are larger than $q_{75} + 1.5\cdot(q_{75} - q_{25})$ or smaller than

Table 4
Estimated model parameters of Eqs. (7)–(9).

Parameter name	Value
k_A	4.39×10^{-5}
Ea_A	182 kJ mo^{-1}
k_B	1.01×10^{-3}
Ea_B	52.1 kJ mol^{-1}

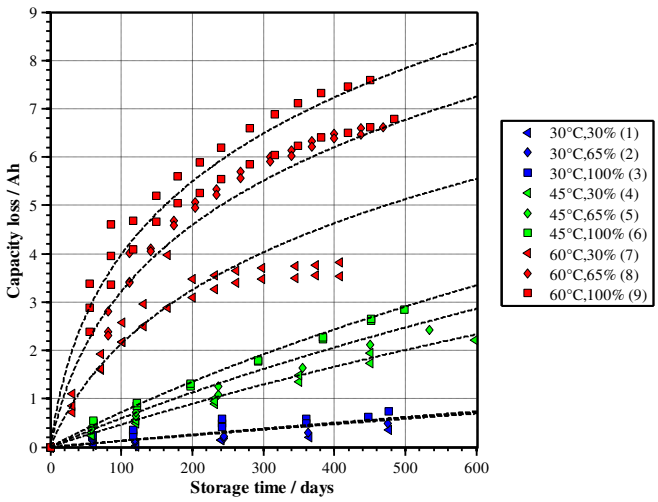

Fig. 8. Fitted degradation model and aging data.

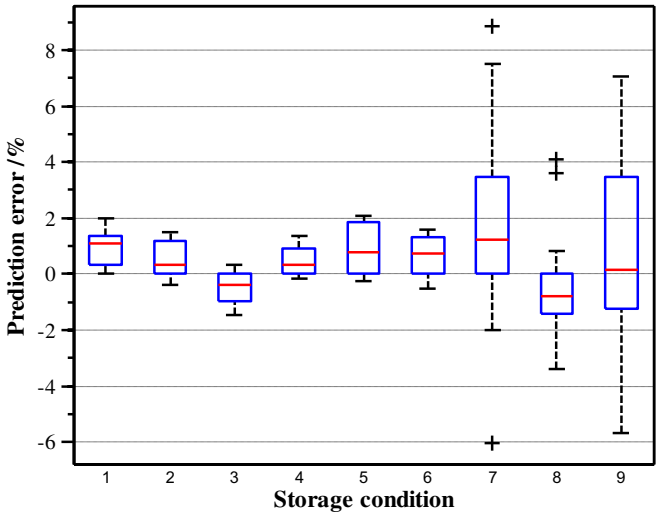

Fig. 9. Distribution plot of capacity prediction error in % for each storage condition.

$q_{75} - 1.5 \cdot (q_{75} - q_{25})$, where q_{25} and q_{75} are the 25th and 75th percentiles, respectively. Mean errors of predicted capacity are equal or very close to 0% for all storage conditions and q_{25}, q_{75} are less than 2% for all storage conditions at 30 °C and 45 °C. Higher error values obtained for the three last conditions ($T = 60$ °C) are easily explained by the relative high discrepancy of data collected for theses extremely severe conditions. Nevertheless, even for these conditions, edges of the box are respectively between −4% and 2% which are satisfactory results.

Finally, estimations of cell lifetimes using the presented model for lower temperatures are reported on Table 5. The temperature and SoC is assumed to have constant values. SoC is fixed to 100% but, as previously stated, below 30 °C, influence of SoC upon storage predicted by our model is minor. At 20 °C, the model predicts that cells can be stored upon 20 years which is fully compatible with electric transportation. However, increasing temperature from 20 °C to 30 °C cuts in half the expected life of the cells.

Table 5
Estimated end-of-life of the cells for different storage temperatures.

Storage temperature	20 °C	25 °C	30 °C
Estimated end-of-life (years)	20	13.5	9

3.3. Validation against non-static storage conditions

The proposed model framework allows simulating degradation induced by storage under non-static conditions by using the derivative form Eq. (4). Thus, degradation induced by the daily temperature profile ("thermal cycling") presented in Section 2.1 was simulated using parameter values from Table 4 for 625 days. To ensure a sufficient precision, a maximum time step of 1 h was allowed.

Fig. 10 compares evolutions of capacity loss measured during successive characterization tests (markers) for thermal cycling conditions (T30//45 °C) and simulated SoH (broken lines). Experimental values and simulation results for static temperature environments 30 °C and 45 °C at the same SoC are also displayed. Amongst the 6 tested cells under thermal cycling conditions, one cell exhibited a faster capacity decline for storage condition 30%. Such unpredictable rapid capacity decline has been already observed for three cells submitted to static storage conditions as reported in Section 3.1.1. Only values of five cells are therefore reported. Measured capacity loss of the remaining cells exposed to thermal cycling lies between those measured on cells stored in static temperature environments 30 °C and 45 °C for both conditions. Scattering between cells is larger for cells under thermal cycling without obvious explanation. The simulated responses of the model agree very well with the experimental data for non-static storage conditions. According to Fig. 11, capacity prediction error lies between −5% and 3% over all 625 days of aging for all cells submitted to thermal cycling.

Although limited to only two non-static storage conditions, the relative good agreement between our measures and our predictions tends to comfort the assumption that the current degradation rate depends only on storage conditions and on the SoH and not on the history of aging. In such case, no detailed history is required to predict future capacity degradation.

4. Conclusion

27 commercial 15 Ah C/LFP cells were stored under nine static different conditions: three temperatures (30 °C, 45 °C, and 60 °C) and three nominal state of charge (30%, 65%, and 100%). Beside pure static temperature conditions, 6 identical additional cells were stored in a controlled 30 °C–45 °C variable temperature environment at two different nominal SoCs (30% and 100%). Degradation of the cells (capacity loss and resistance increase) was periodically monitored by non-destructive electrochemical characterizations. Storage temperature has a strong impact on degradation rate and SoC of storage is of secondary importance compared to storage temperature, but its influence increases with temperature. Fully charged cells stored at 45 °C experienced a capacity loss of 20% within 450 days. All cells stored at 60 °C experienced a minimum of 20% capacity loss within 150 days. Cell resistance derived from discharge current pulses exhibits moderate increase which has no significant impact on the available energy at $1C_{nom}$ discharge rate and at 25 °C, even for severely aged cells. These observations derived from non-destructive characterization are fully compatible with the loss of cyclable lithium due to SEI layer growth which has been previously reported for this cell chemistry submitted to calendar aging.

Parameters of a simple empirical rate-based model predicting capacity fade upon storage have been derived from collected

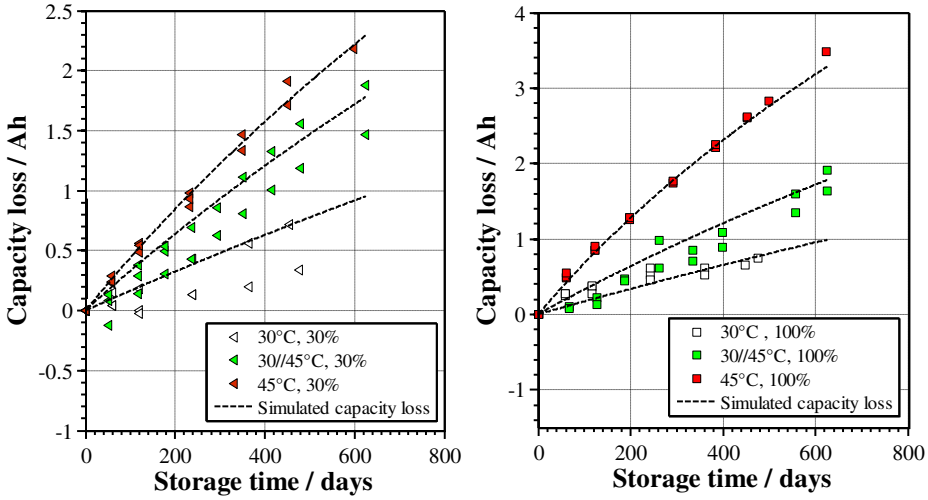

Fig. 10. Capacity loss evolution with storage time for static temperature conditions 30 °C and 45 °C and for thermal cycling aging tests (T = 30//45 °C) at SoC = 30% (left) and SoC = 100% (right) Experimental data (markers) and model prediction (broken lines).

aging data. The model frame was specifically chosen to allow simulating degradation performance upon storage in time variable conditions (SoC and temperature). Predictions of capacity fade (SoH) were compared to experimental data of additional cells stored in a controlled 30 °C–45 °C variable temperature environment. Considering scattering due to aging, the prediction error on cell capacity over 625 days of storage lies between −5% and +3%. Good agreement between prediction and capacity loss comforts the assumption that the capacity fade rate depends only on storage conditions and not on the history of aging. In such case, no detailed history is required to predict future capacity degradation.

The proposed model allows to simulate under various conditions and to estimate degradation upon storage over time. A promising use of such model consists in evaluating the impact on the battery life of different thermal and SoC management strategies upon storage. Ought to the fact that knowledge of the detailed chemistry is not required, our approach is expected to capture rapidly diverse lithium-ion battery technologies.

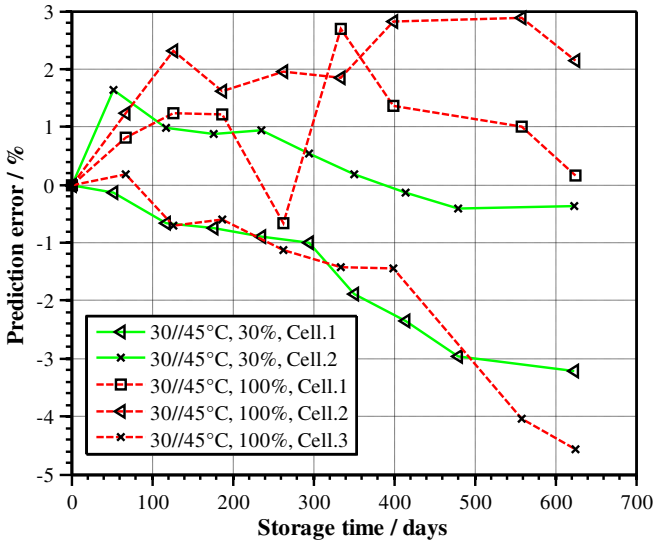

Fig. 11. Capacity prediction error of cells submitted to the thermal cycling.

Acknowledgments

The authors acknowledge funding of this work from University Caen Basse-Normandie. The SIMCAL research network includes 14 partners, namely 8 research labs and affiliated and 6 industrials. The SIMCAL research program aims to study and to understand the calendar aging mechanisms of a wide variety of new battery technologies. The 3.6 M€ cost of the SIMCAL program was shared by 14 French partners including research labs, automakers and one battery manufacturer, with the support of the French National Research Agency ANR. The Laboratory for Electrical Storage (CEA/LSE) is operated by the French Alternative Energies and Atomic Energy Commission.

SIMCAL network partners who have participated:

- CEA: B. Crouzevialle, A. Delaille, S. Grolleau, S. Mailley, B. Molina-Concha
- EDF: L. Jamy
- EIGSI: F. Duclaud, A. Guignard, A. Mieze
- IFP Energies Nouvelles: J. Bernard, R. Revel, F. Moreau, I. Clémençon, D. Audigier, F. Badin, F. Le-Berr, V. Sauvant-Moynot
- IFSTTAR/LTE: S. Pélissier, J. Peter, E. Redondo Iglesias
- IMS: J.M. Vinassa, O. Briat, A. Eddahech, H. Henry
- LEC-UTC: C. Forgez, G. Friedrich
- LMS-Imagine: J. Hafsaoui, P. Aubret
- LRCS: M. Morcrette, C. Delacourt, M. Kassem
- MTA Plateforme d'essais: C. Adès
- PSA Peugeot Citroën: D. Porcellato, M. Capelle, T. Prenant, S. Joly
- RENAULT: P. Gyan
- SAFT: S. Bourlot, P. Blanchard
- VALEO: M. Ouattara-Brigaudet, D. Benchetrite

References

[1] R.P. Ramasamy, R.E. White, B.N. Popov, J. Power Sources 141 (2005) 298.
[2] M. Broussely, S. Herreyre, P. Biensan, P. Kasztejna, K. Nechev, R. Staniewicz, J. Power Sources 97–98 (2001) 13.
[3] J. Belt, V. Utgikar, I. Bloom, J. Power Sources 196 (2011) 10213.
[4] R.B. Wright, C.G. Motloch, J.R. Belt, J.P. Christophersen, C.D. Ho, R.A. Richardson, I. Bloom, S.A. Jones, V.S. Battaglia, G.L. Henriksen, T. Unkelhaeuser, D. Ingersoll, H.L. Case, S.A. Rogers, R.A. Sutula, J. Power Sources 110 (2002) 445.
[5] M. Kassem, J. Bernard, R. Revel, S. Pélissier, F. Duclaud, C. Delacourt, J. Power Sources 208 (2012) 296.

[6] K. Amine, J. Liu, I. Belharouak, Electrochem. Commun. 7 (2005) 669.
[7] R.V. Bugga, M.C. Smart, L. Whitcanack, ECS Trans. (2010) 297–306.
[8] J. Vetter, P. Novák, M.R. Wagner, C. Veit, K.-C. Möller, J.O. Besenhard, M. Winter, M. Wohlfahrt-Mehrens, C. Vogler, A. Hammouche, J. Power Sources 147 (2005) 269.
[9] P. Arora, R. White, M. Doyle, J. Electrochem. Soc. 145 (1998) 3647.
[10] M. Broussely, P. Biensan, F. Bonhomme, P. Blanchard, S. Herreyre, K. Nechev, R.J. Staniewicz, J. Power Sources 146 (2005) 90.
[11] M. Safari, C. Delacourt, J. Electrochem. Soc. 158 (2011) A1123.
[12] K. Edström, M. Herstedt, D.P. Abraham, J. Power Sources 153 (2006) 380.
[13] R. Yazami, Y. Reynier, Electrochim. Acta 47 (2002) 1217.
[14] M. Broussely, Ageing Mechanisms in Li-ion Batteries and Life Predictions, n.d.
[15] E. Peled, J. Electrochem. Soc. 126 (1979) 2047.
[16] M. Dubarry, B.Y. Liaw, J. Power Sources 194 (2009) 541.
[17] A.K. Padhi, J. Electrochem. Soc. 144 (1997) 1188.
[18] K. Striebel, A. Guerfi, J. Shim, M. Armand, M. Gauthier, K. Zaghib, J. Power Sources 119–121 (2003) 951.
[19] Y. Zhang, C.-Y. Wang, X. Tang, J. Power Sources 196 (2011) 1513.
[20] P. Liu, J. Wang, J. Hicks-Garner, E. Sherman, S. Soukiazian, M. Verbrugge, H. Tataria, J. Musser, P. Finamore, J. Electrochem. Soc. 157 (2010) A499.
[21] J. Wang, P. Liu, J. Hicks-Garner, E. Sherman, S. Soukiazian, M. Verbrugge, H. Tataria, J. Musser, P. Finamore, J. Power Sources 196 (2011) 3942.
[22] M. Safari, C. Delacourt, J. Electrochem. Soc. 158 (2011) A1436.
[23] M. Kassem, C. Delacourt, J. Power Sources 235 (2013) 159.
[24] M. Safari, M. Morcrette, A. Teyssot, C. Delacourt, J. Electrochem. Soc. 157 (2010) A713.
[25] P. Ramadass, B. Haran, P.M. Gomadam, R. White, B.N. Popov, J Electrochem. Soc. 151 (2004) A196.
[26] H.J. Ploehn, P. Ramadass, R.E. White, J. Electrochem. Soc. 151 (2004) A456.
[27] R. Spotnitz, J. Power Sources 113 (2003) 72.
[28] M. Safari, M. Morcrette, A. Teyssot, C. Delacourt, J. Electrochem. Soc. 156 (2009) A145.
[29] E. V Thomas, H.L. Case, D.H. Doughty, R.G. Jungst, G. Nagasubramanian, E.P. Roth, J. Power Sources 124 (2003) 254.
[30] I. Bloom, B.W. Cole, J.J. Sohn, S.A. Jones, E.G. Polzin, V.S. Battaglia, G.L. Henriksen, C. Motloch, R. Richardson, T. Unkelhaeuser, D. Ingersoll, H.L. Case, J. Power Sources 101 (2001) 238.
[31] K. Smith, G.-H. Kim, A. Pesaran, Presented at the 215th Electrochemical Society Meeting, 25–29 May 2009, San Francisco, CA, 2009.
[32] E.V. Thomas, I. Bloom, J.P. Christophersen, V.S. Battaglia, J. Power Sources 206 (2012) 378.